A multi-technique comparison of the electronic properties of pristine and nitrogen-doped polycrystalline SnO2

Livraghi, S; Barbero, N.; Agnoli, S.; Barolo, C.; Granozzi, G.; Sauvage, F.; Giamello, E.. A multi-technique comparison of the electronic properties of pristine and nitrogen-doped polycrystalline SnO2. PHYSICAL CHEMISTRY CHEMICAL PHYSICS. 18 (32) pp: 22617-22627.
DOI: 10.1039/c6cp02822e

A multi-technique comparison of the electronic properties of pristine and nitrogen-doped polycrystalline SnO_2.

S. Livraghi[1], N. Barbero[1,2], S. Agnoli[3], C. Barolo[1], G. Granozzi[3], F. Sauvage[2], E. Giamello[*1]

1. *Dipartimento di Chimica, Università di Torino and NIS, centre for Nanostructured Interfaces and Surface , Via P. Giuria 7, I - 10125 Torino, Italy*
2. *Laboratoire de Réactivité et Chimie des Solides, Université de Picardie Jules Verne, CNRS UMR 7314, 33 rue Saint Leu, 80039 Amiens, France*
3. *Dipartimento di Scienze Chimiche, Università di Padova, Via Marzolo 1, 35131 Padova, Italy*

Abstract:

Nitrogen doped tin(IV) oxide (SnO_2) materials in the form of nanometric powders have been prepared by precipitation with ammonia. Their properties have been compared with those of undoped materials obtained in a similar way using various physical techniques such as Photoelectron Spectroscopies (XPS and UPS), UV-Vis-NIR spectroscopy and Electron Paramagnetic Resonance (EPR). Nitrogen doping leads to the formation of various nitrogen containing species the more relevant of which is a nitride-type ionic species based on the substitution of a lattice oxygen atom with a nitrogen one. This species exists in two forms, a paramagnetic species (hole centre, formally N^{2-}) and a diamagnetic one (N^{3-}). The mutual ratio of the two species varies according to the oxidation state of the material. The doped solid, like most of semiconducting oxides, tends to lose oxygen forming oxygen vacancies upon annealing under vacuum and leaving excess of electrons in the solid. The stoichiometry of the solid can thus be markedly changed depending on the external conditions. Excess electrons are present both as itinerant electrons in the conduction band and as Sn(II) states lying close to the valence band maximum. The presence of nitride-type centres, which are low energy states located below the top of the valence band, decreases the energy cost for the formation of oxygen vacancies by O_2 release from the lattice. This particular feature of the doped system represents a severe limit to the preparation of a p-type SnO_2 via nitrogen doping

1. Introduction.

Tin (IV) oxide (SnO_2), in spite of a wide band gap of 3.6 eV[1], is an intrinsic n-type semiconductor belonging to the category of transparent conducting oxides (TCO), which has been extensively used for many years mainly in the form of conducting thin films. The insulator to semiconductor transition in SnO_2 is caused by the presence of shallow donor levels near the conduction band. These are, in turn, related to the formation of lattice intrinsic defects. Both experimental and computational studies shows that interstitial tin and oxygen vacancies are easily formed and dominate the defect structure of SnO_2 so explaining the tendency of this material for non-stoichiometry and its properties to maintain *n*-type conduction.[2]

Due to these peculiar properties, tin oxide finds application as chemical sensor,[3] in lithium-ion batteries,[4] and in solar cells.[5] Tin oxide is also employed in heterogeneous oxidation catalysis,[6] while there are only few reports regarding its photocatalytic properties, except for the case of SnO_2-based heterojunctioned photocatalysts[7] and for some recently reported applications in visible light photocatalysis based on band gap tuning via Sn^{2+} self doping.[8-10]

However, SnO_2 in its pristine form, is seldom exploited in practical applications. These in facts generally require that the oxide is modified by doping with the aim of controlling its physical properties. The electrical conductivity, in particular, is modified by the incorporation of either cations or anions bearing an extra electron with respect to Sn and O, respectively (n-type doping). To this purpose, antimony (Sb-SnO_2) and fluorine (F-SnO_2) are the elements of choice in most cases as they afford to combine high electronic conductivity while preserving excellent optical transparency.[11-14]

More recently, and similarly to the case of other oxides like TiO_2 or ZnO,[15-17] the attention of researchers has turned to the problem of p-type doping of SnO_2, mainly pursued by the introduction of nitrogen, an element bearing one electron less than oxygen.[18-32]

Even though the possibility to prepare a p-type SnO_2 represents a questionable topic,[33] the obtaintion of a stable phase of p-type SnO_2 would have a huge impact on the fabrication of various

kind of opto-electronic devices.[21,22,28] Nitrogen doped SnO_2 (hereafter N-SnO_2) has been taken into account, for instance, for the preparation of diluted magnetic semiconductors of potential use for spintronics [23,24,28] and more recently as anode in lithium-ion batteries.[27,30]

Theoretical calculations show that incorporation of N in the O site of the lattice is energetically favourable, while the interstitial N species have large formation energy in both O-rich and Sn-rich growth conditions.[21] Incorporation of N in the SnO_2 lattice also causes photoluminescence emission spectra different from those of the pure material.[19,25] Optical band gap narrowing from UV to visible range has also been reported for this material.[25,28,31]

Recently some of us have used a combination of electron paramagnetic resonance (EPR) spectroscopy and density functional theory (DFT) calculations to characterize the electron spin density of the nitrogen paramagnetic center in N-doped SnO_2 polycrystalline materials prepared by wet chemistry.[32] In the present paper we extend our attention to the characterization of the N-doped material by various physical techniques, aiming to provide a comprehensive description of this discussed system with particular attention to its electronic structure. This will be done comparing the properties of the doped system with those of the undoped one, prepared by the same method.

2. Experimental.

2.1 Materials characterization.

X-ray diffraction (XRD) analysis of SnO_2 nanoparticles was performed using a Bruker D4 diffractometer with Cu K_α radiation. The data were collected in the range from $2\Theta = 20°$ to 75°. The crystallite size was evaluated using the Scherrer method. Transmission electron microscopy images (TEM) were obtained by a high resolution FEG FEI Tecnai F20 S-TWIN with accelerating tension of 200 kV. Diffuse Reflectance Spectroscopy (DR UV-Vis-NIR) was employed to characterize the absorption features in a range of wavelength between UV and NIR (250 – 2500 nm). DR UV-Vis-NIR measurements were performed on fine powders of the samples. The spectra were collected in the reflectance mode with a Perkin-Elmer Cary5000 instrument equipped with an integrating sphere

and then reported as an absorbance-like pattern by means of the Kubelka-Munk function. Optical bandgap absorption was obtained by means of a Tauc plot of the Kubelka-Munk absorption as a function of the photon energy.[34]

X-band Continuous Wave (CW) EPR spectra have been recorded on a Bruker EMX spectrometer equipped with a cylindrical cavity and operating at a 100 kHz field modulation. The measurements were carried out at room temperature (RT) and liquid nitrogen temperature (77 K) in cells that can be connected to a conventional high-vacuum apparatus (residual pressure < 10^{-4} mbar).

Photoemission spectra were acquired in a custom designed ultra-high-vacuum UHV system, working at a base pressure of 10^{-10} mbar, equipped with a VG MK II Escalab electron analyzer, facilities for sample heating up to 1073 K. Core level photoemission spectra (XPS) were taken at RT in normal emission using a non monochromatized Mg K_α X-ray source (1253.6 eV). The spectrometer energy calibration was carried out by using a gold sample (Au 4f at 84 eV). Single spectral regions were collected using 0.1 eV steps, 0.5 s collection time and 20 eV pass energy. Valence band (VB) data (UPS) were collected using a He discharge lamp (HIS 13, Omicron) exploiting the He II radiation line (40.8 eV) and He I (21.2 eV).

2.2 Samples preparation

Both pristine and N-doped SnO_2 nanoparticles were synthesized by a wet chemistry method using tin metal as a precursor. In a typical synthesis procedure,[35] 5 g of granulated tin and 15 g of citric acid were dissolved completely in 8 M nitric acid under vigorous stirring. Aqueous ammonia was added drop-wise to the resulting solution to pH = 8.0. The resultant solution was refluxed at 373 K for 2 hours. After cooling down, the solution was centrifuged at 6000 rpm for 1 hour and the ensuing sol was collected and washed repeatedly with ethanol. It was then dried in oven at 333 K for 15 hours. The undoped counterpart was synthesized according to a very similar procedure, using only NaOH instead of ammonia to obtain a pH of 8.0. Both doped and undoped materials were finally calcined in a range of temperature between 773 K and 973 K. The resulting powders are

yellow for N-doped SnO_2 (SN1, SN2, SN3 samples) by contrast to the typical white coloration for undoped SnO_2 (S1, S2, S3 samples). Table 1 resumes the main features of the samples prepared in this work.

Sample abbreviation	Alkaline agent	Calcination Temp. (K)	Phase	Crystallite size (nm)	Band gap* (eV)	colour
S1	NaOH	773	Cassiterite	3.9	4.0	white
S2	NaOH	873	Cassiterite	4.2	3.9	white
S3	NaOH	973	Cassiterite + Na_2SnO_3	4.5	3.9	white
SN1	NH_3	773	Cassiterite	7	3.7	yellow
SN2	NH_3	873	Cassiterite	10	3.8	yellow
SN3	NH_3	973	Cassiterite	15	3.8	yellow

Table 1: Abbreviation adopted for the samples employed in this work and the corresponding structure, crystallite size and optical bandgap values. * Band gap values derived from optical spectra (Tauc plot).[34]

3. Results and discussion:

3.1 Structural, morphological and optical characterization of SnO_2 and N-SnO_2.

The X-ray diffraction patterns of the six samples considered are shown in Fig.1. All samples show the characteristic diffraction peaks of the tetragonal Cassiterite structure of SnO_2. In the case of the undoped material calcined at the highest temperature (973 K), onset of a few additional diffraction peaks can be observed, tentatively attributed to sodium stannate (Na_2SnO_3) which may stems from residual sodium hydroxide reacting with the tin precursor or the already formed tin oxide. The undoped materials (Fig. 1, Panel A) show broader diffraction peaks compared to the corresponding N doped samples (Fig. 1, Panel B), indicating a smaller crystallite size. As one could expect, calcination at high temperature leads to a narrowing of the diffraction peaks as a result from grain size coarsening. Interestingly, this is much more evident in the doped materials for which the crystallite size lies between 7 to 15 nm as deduced by using the empirical Scherrer formalism. By comparison, using rigorously the same synthetic procedure, the crystallite size for the undoped SnO_2 remains from 3.9 to 4.5 nm. Interestingly, this tends to demonstrate that particles coarsening

process is favored when nitrogen is included inside the lattice. The same observation also indicates that the surface energy contributing to the total free Gibbs energy of the Cassiterite structure becomes preponderant at a size threshold of *ca.* 4 nm thus contributing to both the higher thermal stability of the crystal structure and the hindrance of particles growth. This finding falls perfectly in line with a recent report describing the thermodynamic frustration on ultra nano-sized anatase TiO_2 system.[36] The morphology of the particles is also different depending on whether there is nitrogen doped or not. The temperature of calcination does not influence noticeably the particles morphology. N-SnO_2 shows particles with hexagonal shape whereas the undoped counterpart are more spherical to rectangular in shape. High resolution images shows that the particles are single crystals without any occurrence of amorphous or disordered region. EDS measurements on N-SnO_2 shows the presence of nitrogen in addition to the SnO_2 signal whereas Energy Filtered Transmission Electron Microscopy (EFTEM) experiments suggested that nitrogen atoms are uniformly distributed inside the sample.

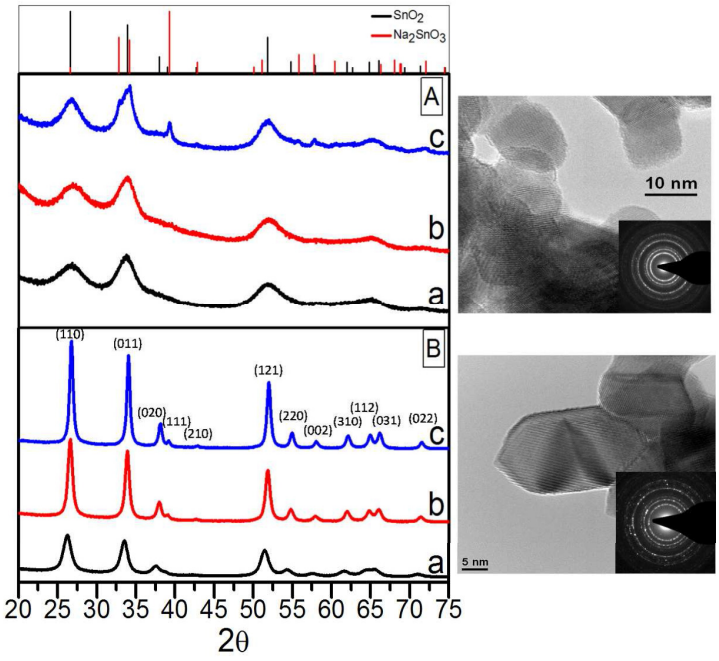

Fig. 1 X-ray diffraction patterns including a representative example of high resolution image by transmission electron microscopy of: Panel A: bare SnO_2 , a) S1, b) S2, c) S3. Panel B: N-doped SnO_2 a) SN1, b) SN2, c) SN3.

Tin oxide is a white material for which a bandgap value of 3.6 eV is usually reported, corresponding to an absorption threshold in the UV region ($\lambda < 340$ nm).1 However, in the present work, depending on the adopted precipitation agent (NaOH or NH_3 solutions), the final materials show different optical properties. Samples obtained using sodium hydroxide are almost white as expected, whereas the materials obtained using ammonia appear yellow.

To better insight on this color aspect modification, in figure 2 the DR-UV-Vis-NIR spectra recorded in various ranges of wavelength are reported for both SnO_2 (left-hand panels) and N-SnO_2 (right-hand panels). Looking at the complete range between 250 nm and 2500 nm, the optical properties of the two materials (panels A and A') appears relatively similar. However, looking more closely to the bandgap transition region (Panels B and B'; 250nm – 600 nm) and to the NIR region (Panels C and C'; 750nm – 2500 nm), one can notice some differences between the two set of materials.

First the band gap values, determined by using the Tauc plot method, are systematically larger than the value of 3.6 eV reported in the literature (see Table 1). The calcination temperature exerts a slight influence on this value (Panels B and B'). This anomaly bandgap increase has been already observed in the case of SnO_2 or TiO_2 and has been ascribed to the Burstein-Moss effect resulting from the presence of free-electrons populating the bottom of the conduction band (CB).[37,38,39] This attribution is also supported by the drift of the optical absorption in the NIR to higher wavelength.

This effect is the consequence of the presence of oxygen vacancies, formed by oxygen depletion from the oxide, and to the subsequent excitation in conduction band of the electrons left in the solid:

1) $O^{2-} \rightarrow ½\ O_2 + V_O^x$

The Kröger-Vink equation above illustrates the formation of an oxygen vacancy filled by two electrons (hence neutral) through O_2 withdrawing from the solid. The trapped electrons constitute shallow levels in the bandgap from which they are easily excited in the conduction band (CB).

2) $V_0^x \rightarrow V_0^{\bullet} + e^-(CB)$

3) $V_0^{\bullet} \rightarrow V_0^{\bullet\bullet} + e^-(CB)$

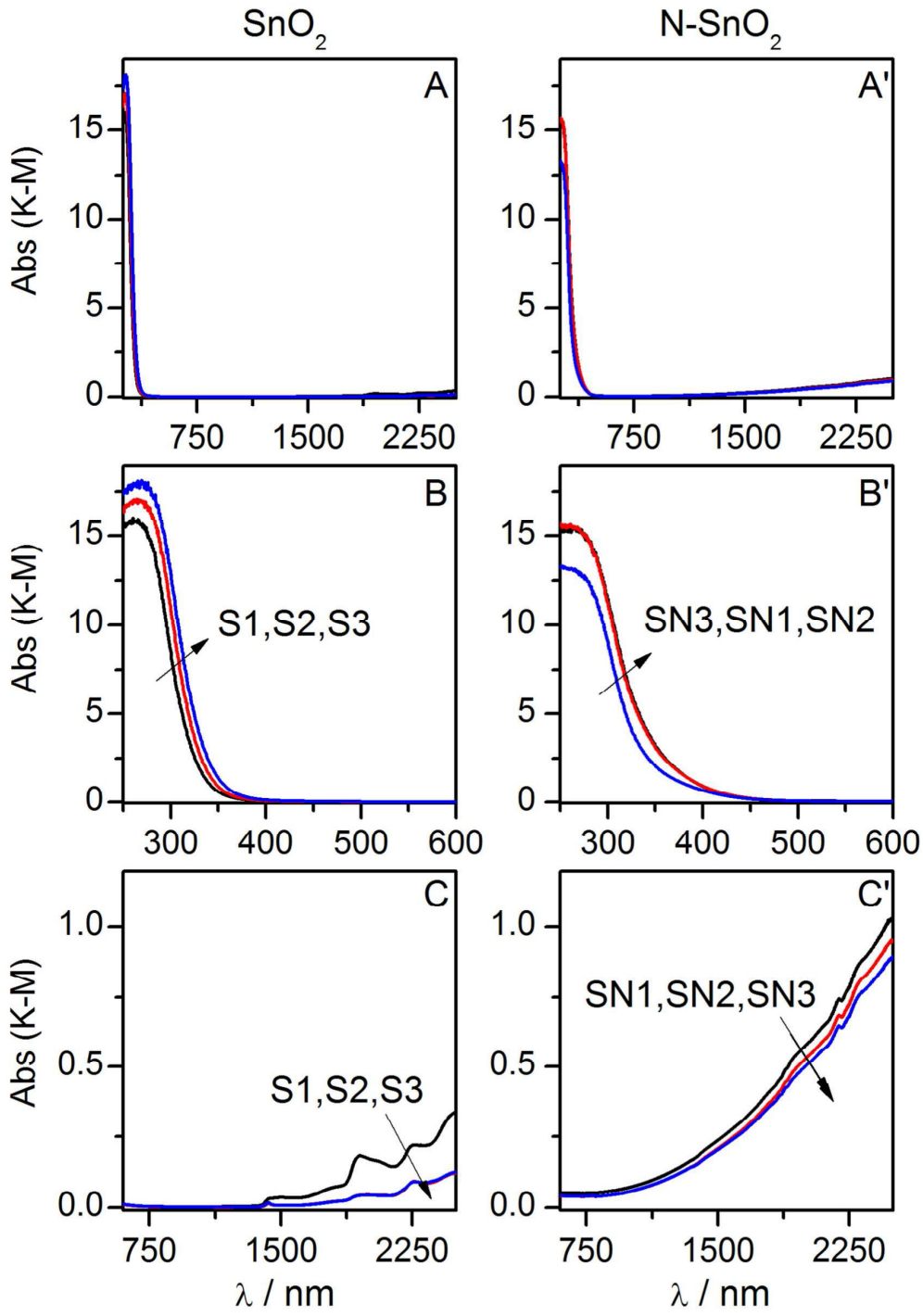

Fig. 2. DR-UV-Vis-NIR spectra of SnO_2 (A, B, C panels) and N-SnO_2 (A', B', C') as-prepared samples after calcination at three different temperatures (see Table 1) in the wavelength range 250nm -2500nm. Panels A and A': full range. B and B': band gap transition region. C and C': NIR region.

The optical absorption in the NIR region is mainly due to the itinerant electrons in the conduction band (Drude absorption).[40] Remarkably, this kind of absorption, approximately proportional to the amount of electrons present in the CB, is systematically higher in the case of N doped materials.

The yellow color observed for N-SnO_2 results from the pronounced tail of the bandgap transition towards the visible region (400 nm – 500 nm) which is absent in all bare materials (Panels B and B').

The optical properties shown in Fig. 2 are those of the materials after calcination in air and are affected, as discussed before, by the presence of some oxygen vacancies with consequent excitation of electrons in CB. This corresponds to a given degree of reduction (or of non-stoichiometry) of the system with respect to the stoichiometric formula. The system, after calcination, has thus attained an equilibrium with its environment. As in the case of other semiconducting oxides, this equilibrium can be modified by oxidative or by reductive treatments carried out at high temperature under O_2 or vacuum, respectively. As shown in Fig. 3 for N-SnO_2, the thermal treatments induce a coherent modification of the Drude-type absorption in the NIR. Upon annealing under vacuum the reduction degree of the material grows and the number of itinerant electrons (hence of oxygen vacancies) increases. By oxidation at 773 K, the drift of the absorption vanishes and is relieved by a flat line indicating that the concentration of itinerant electrons has been radically decreased by the treatment. The thermal treatments above described not only affect the optical features in the NIR region but also induce a modification of the absorption tail of the band gap transition (Fig. 3b and 3c). Similarly to the absorption in the NIR region, such feature (absorption in the range 500-700 nm) increases upon annealing in vacuum and decreases after oxidation. Such behavior clearly indicates that, beside the formation of itinerant electrons, new energy states strictly related to the reduction degree of the material are also generated close to the valence band in N-SnO_2. As it will be discussed in the following (Section 3.3) this behavior is due to the presence of Sn(II) states located above the valence band and formed upon reduction. To summarize, the non-stoichiometry degree (or reduction degree) indicated by the NIR absorption is higher for N-SnO_2 than for the

undoped material under equal conditions. The reduction degree, as expected can be modified upon treatments under oxygen or upon annealing in vacuum at high temperatures and markedly affects the optical properties of the material both in the visible and NIR regions.

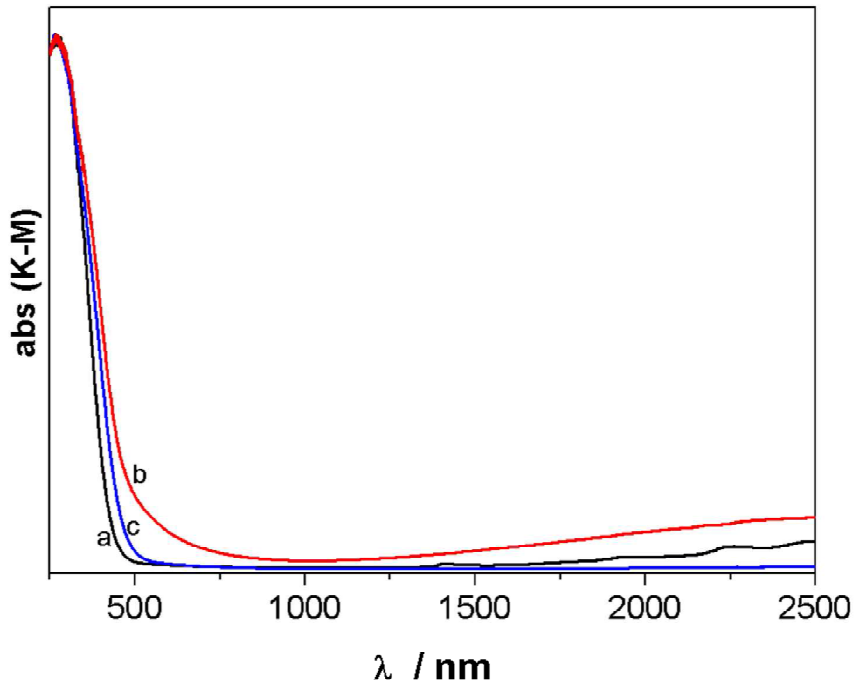

Fig. 3. DR-UV-Vis-NIR spectra SN1 sample a) as-prepared samples (see Table 1). b) after annealing under vacuum at 773K. c) after oxidation in O_2 at 773K.

3.2 EPR characterization.

The EPR investigation of N-SnO_2 provides two main information that are illustrated in the following. The first one is that EPR signals due to N-containing paramagnetic species are observed in the doped material. The second information is that the effects of the non-stoichiometry described above for the NIR absorption, also affect the EPR spectra. Figure 4a shows the spectrum of the as prepared material SN1 material (calcined at 773 K) recorded at 77 K, which results from the overlap of two distinct signals. The first one (species A) is observed at the liquid nitrogen temperature only (77 K) and is a rhombic signal whose main feature is a ^{14}N hyperfine triplet with

3.2 mT separation centered at g=2.003. Signal A is well known from the literature and its structure is that expected for nitric oxide (NO, a $11e^-$ diatomic π-radical) absorbed on a cationic (Sn^{4+}) site.[41] Considering that the NO signal is observed at low temperature only (77 K) and is not affected by outgassing the material at RT, it can be concluded that NO is trapped in microvoids present in bulk of N-SnO_2 microcrystals as already reported for similar oxides.[42,43] As in other cases like TiO_2, the presence of this species represents a byproduct of the preparation method due to the oxidation of ammonia during calcination.[44] A similar signal, was reported in the case NO absorption on SnO_2.[45,46]

The second feature (Signal B) of Fig. 4a is a relatively broad symmetric signal (5 mT of peak-to-peak linewidth) centered at g=1.89 and well known from the EPR investigations of SnO_2, [47,48,49] which is due to single electrons trapped in oxygen vacancies ($V_0^{\bullet}$). The energy level of this center, as well as that of the two-electron diamagnetic center (V_0^{x}), is very close to the edge of the CB so that the trapped electron is easily thermalized in such a band. This explains the somehow erratic trend of the intensity of this signal in the various samples examined in the present work.

After an oxidative treatment directly performed in the EPR cell and consisting of an evacuation at 773 K followed by an oxidation in 20 mbar O_2 at the same temperature for one hour both signals in Fig. 4a vanish and a new more complex spectrum shows up (Species C, Fig. 4b). This is observed both at RT and low temperature (77 K) and is characterized by rhombic symmetry with a weakly anisotropic $\boldsymbol{g}$ tensor (g_1 = 2.0053, g_2 = 2.0023, g_3 = 1.9978) and by a complex hyperfine structure owing to ^{14}N (A_1(N) = 4.17 mT, A_2 (N) = 0.08 mT, A_3 (N) = 0.08 mT) and to the two more abundant tin isotopes having non-zero nuclear spin, ^{117}Sn and ^{119}Sn (having natural abundance of 7.75% and 8.6% respectively). The detailed analysis of this complex signal has been the object of a specific paper[32]. In that paper it was possible to assign the paramagnetic species responsible of the spectrum to a nitrogen paramagnetic centre substituting oxygen ($N_{sub.}$) in the lattice of the oxide.[32] In formal terms the centre can be described as a 9-electrons N^{2-} centre. The unpaired electron is in a p-orbital of nitrogen with a strong degree of localization. Table 2

summarizes the main spin Hamiltonian parameters of the two paramagnetic species formed in N-SnO_2.

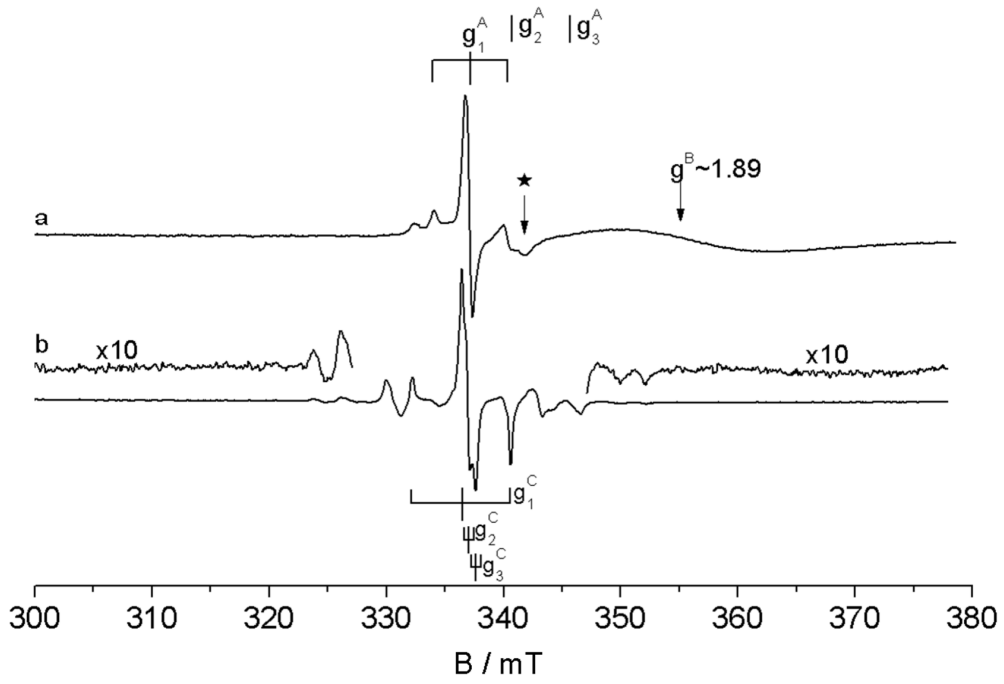

Fig. 4 Normalized CW-EPR spectra of N-SnO_2 recorded at 77K, a) as prepared N-SnO_2 b) N-SnO_2 after oxidative thermal treatment. Upper stick diagram identify the **g** and **A** tensors of species A (trapped molecular NO) whereas the lower one identify the g and A tensors of species B. The star indicates a spurious species.

The EPR signal of N_{sub} (Fig. 4b) has been also recorded under irradiation in order to verify whether the electrons of the N species can be photo-excited as it occurs, for instance, in the case of analogous centres in TiO_2.[15,50] In that case a behaviour typical of an intra band gap energy level was observed with the intensity of the signal that is selectively modified by light of specific wavelengths; either because of excitation of the single electron in CB[50] or because of electron pairing by excitation from the VB[15]. The behaviour of the N_{sub} paramagnetic centre in SnO_2 (Fig. 4b) is different since its intensity remains constant under all type of irradiation from UV to visible. This result is in agreement with what has been derived from DFT calculations showing that the electronic level of the N centre lies underneath the top of the valence band (and not in the bandgap) so that a direct specific photoexcitation of the electrons of the centre is impossible.[32]

Interestingly, however, the intensity of the N_{sub} signal gradually vanishes if the sample is exposed to the atmosphere. This occurs while the solid attains a new equilibrium with atmosphere loosing oxygen and producing excess electrons. A new oxidative treatment at high T is necessary to recover the original intensity of the signal. To summarize, the most important paramagnetic species characterizing N-SnO_2 is a N^{2-} ion (N_{sub}) that substitutes an oxygen ion in a regular lattice position and whose electronic state (SOMO) lies at an energy corresponding to the VB range. This prevent the direct photoexcitation of the electron. The paramagnetic state is observed only in fully oxidized samples, while in reduced, electron richer, states it is transformed in a paramagnetic entity likely because of electron scavenging (see below).

Species	g_1	g_2	g_3	A_1 (mT) (N)	A_1 (mT) (N)	A_1 (mT) (N)	A_1 (mT) (^{117}Sn)	A_1 (mT) (^{117}Sn)	A_1 (mT) (^{117}Sn)	Ref.
NO	2.003	2.001	1.954	<0.3	3.2	0.6	-	-	-	This work
$N_{sub.}$	2.005	2.002	1.998	4.2	0.1	0.1	11.7	12.3	11.9	32 and this work
N_i in TiO_2	2.005	2.004	2.003	0.2	0.4	3.2	-	-	-	50
NO in TiO_2	2.003	1.998	1.927	<0.1	3.2	1	-	-	-	42
NO on SnO_2	2.001	1.998	1.95	0	~3	0	-	-	-	46

Table 2: Spin Hamiltonian parameters of paramagnetic nitrogen species in N-SnO_2 and comparison with similar cases.

3.3 XPS/UPS characterization.

Shown in Fig. 5 are the N(1s) photoemission spectra of the SN1 sample before and after thermal annealing in ultra-high vacuum at different temperature for 15 min (10 minutes to reach the temperature, 15min at the set temperature and 15 min for cooling down). The N1s photo-emission line is rather large indicating the presence of different chemical states and structural environments for the nitrogen species at the surface and inside the SnO_2 matrix.

A systematic multi-peak analysis of these spectra indicates the presence of two families of peaks, the former with binding energy (BE) components at 397.1 and 398. 3 eV, the second with peaks ranging from 399.4 eV to 400.7 eV.

The first family with lower binding energies can be associated with the presence, in the SnO_2 lattice, of nitride species,[51,52] while binding energy with higher value (399.4–403.2 eV) correspond to different N bonding structures including NO_x –type compounds.

The thermal annealing *in vacuo* induces a decrease of the oxygen fraction in the solid as determined in terms of the O 1s peak, for which the intensity drops to about 5%. It also leads to an overall increase of the amount of N detected by photo-emission (1.9 % at room temperature and about 3% for higher temperature treatments). This is accompanied by a modest increase of the nitride-like components with respect to more oxidized NO_x species. For this reason, these are supposed to be preferentially localized at the surface.

A quantitative analysis of the surface and sub-surface regions accessible to X-rays has been also performed in the case of the as-prepared SN1 material obtaining an (O+N)/Sn atomic ratio of 1.88. Such value suggests that, despite the final calcination at 773 K and as indicated by the spectra in Fig.2 C', the N containing as prepared material is oxygen deficient and rich of oxygen vacancies ($SnO_{2-x}N_y$).

Since the discrimination between Sn^{2+} and Sn^{4+} by photoemission measurements on the Sn 3d level is quite difficult, we have resorted to the investigation of the valence band by UPS.1 In figure 6 the UPS (Ultraviolet Photoemission Spectroscopy) data for the as prepared SN1 sample acquired using the He (II) emission line ($h\nu$=40.8 eV) as exciting radiation, are compared with those of S1 progressively annealed at increasing temperature. UPS is able to investigate the valence band spectra near the Fermi level, allowing to monitor the electronic structure of the materials. The UPS spectrum of the doped as-prepared SN1 material shows three well defined bands at about 4 eV, 7 eV and 11 eV which are the typical fingerprint of SnO_2[4,53] accompanied by a weaker shoulder at around 2 eV.

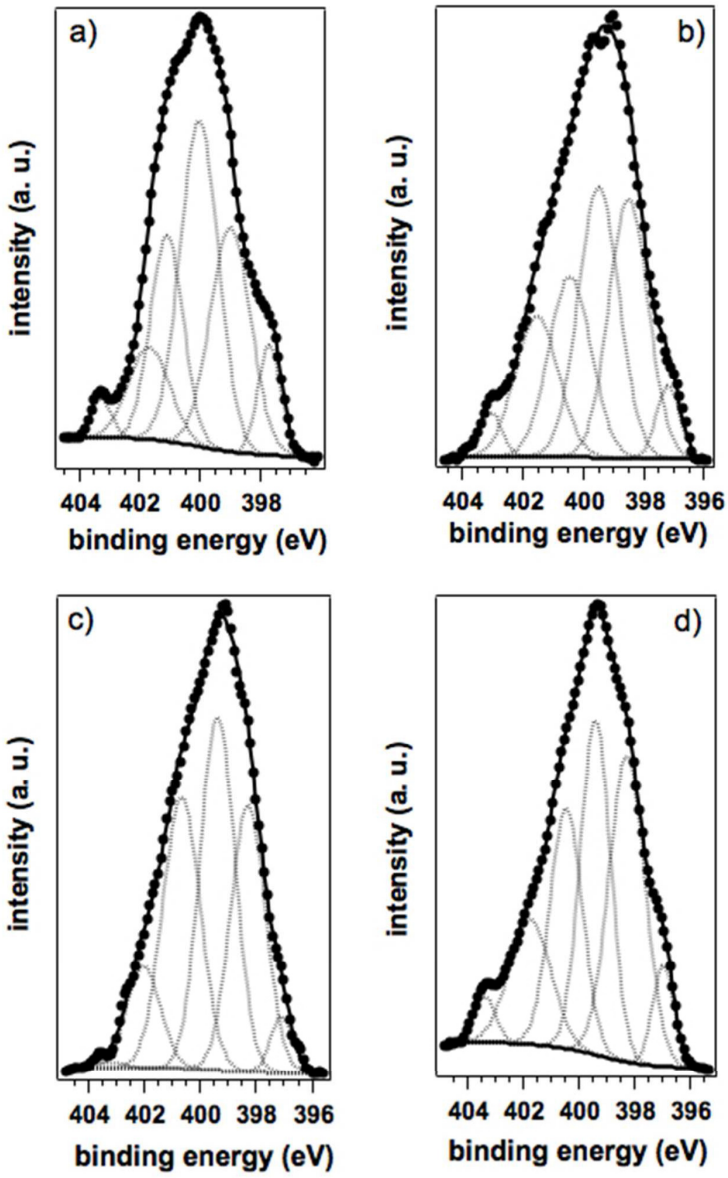

Fig. 5 N(1S) XPS data of SN1 sample as prepared (a) and after annealing under UHV at 923 K (b), 1023K (c) and 1123 K (d).

The initial spectrum of S1 (as prepared, Fig 6a) is broad and featureless probably because of the smaller crystal size of this material and the presence of some adsorbates. The valence band maximum (VBM), estimated via interpolation of the slope of the valence band and using its intercept with the energy axis, results to be about 3.0 eV below the Fermi level, for the S1 sample

and 3.4 eV for SN1 indicating that, surprisingly and in spite of the introduction of a p-type dopant the N doped SnO_2 continues to maintain a strong n-type character.

The relatively weak peak at about 2 eV shown by the calcined SN1 sample (Fig. 6d) is however relevant to the discussion relative to the electronic structure of this material. This feature is usually assigned to the presence of Sn^{2+} ions in the system.[53] The dual valence of tin and the stability of a divalent oxide (SnO) is well-known. Furthermore, since Sn^{4+} and Sn^{2+} have similar radius, the latter ion can be easily hosted in the SnO_2 matrix minimizing the structural deformation.[8,9,10]

The presence of Sn^{2+} states close to the valence band of the solid is reminiscent of what occurs when moving from SnO_2 to SnO. In fact, the 5s levels of tin, which are empty and constitute the bottom of the CB in SnO_2, host an electron pair in the case of Sn^{2+} and become the top of the VB of SnO. The assignment of the 2 eV peak to Sn(II) is confirmed by the spectra in Fig. 6 (from b to d) that show the effect of the gradual (reducing) annealing at increasing temperature of the S1 sample. The ongoing oxygen depletion induces the formation of oxygen vacancies (V^{x}_{O} equation 3) a fraction of which, at least, transfer electrons to Sn^{4+} according to equation 4.

3) $SnO_2 \rightarrow SnO_{2-x} + \frac{1}{2}\, xO_2 + xV_0^x$

4) $V_0^x \rightarrow V_0^{\bullet\bullet} + 2e^-$; $Sn(IV) + 2e^- \rightarrow Sn(II)$

The thermal reduction process in Fig. 6(a-d) is accompanied by the growth of a new feature above the VBM with 2 eV of binding energy. This same band is already visible in the VB spectrum of SN1 even in the case of the initial calcined material (Fig. 6d) meaning that it already contains reduced tin ions. This observation is confirmed by two further evidences. The former one (Fig. 7) is based on the difference in binding energy observed comparing the XPS (Sn, 4d peak) for the as-prepared doped and undoped materials, respectively.

The small, but net shift between the two BE values indicates a difference in the average oxidation states of tin in the two materials.[53] The second evidence is resumed in Fig. 8 that compares the UPS valence band spectra of the N-doped SN1 material acquired by using two different excitation energy (He(I) and He(II) respectively). The comparison of the two spectra allows to exclude a

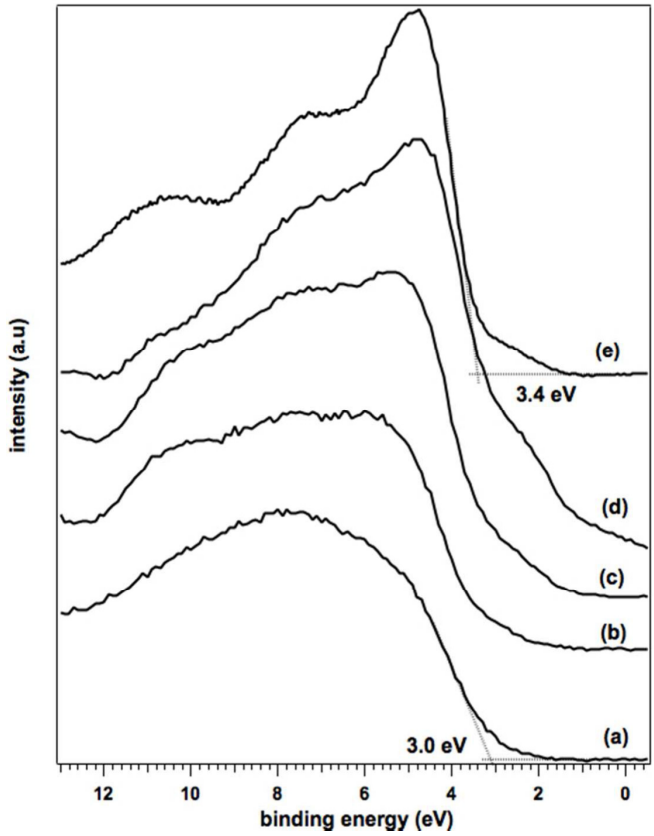

Fig. 6 UPS data of as prepared S1 (a) and of the same sample annealed in UHV at 623 K (b), 703 K (c), 823 K (d). e) as prepared SN1. Each step of annealing was performed for 15 min.

predominant role of nitrogen in the component at 2 eV. If it were so, in fact, the change of the exciting radiation energy passing from He(I) to He(II) would cause a significant decrease (30%) of the N 2p cross section with dramatic lowering of the intensity of this component with respect to that at 4.5 eV (associated with O 2p levels),[53,54] and this is not the case (Fig. 8), whereas for Sn 5s the effect would be in the opposite direction (5 times increase). Experimentally only a mild intensity gain is observed, much lower than what would be expected for a purely Sn 5s, meaning that this band likely could comprise some contamination by N 2p levels.Summarizing, XPS and UPS experiments indicate that a nitride species is present in N-SnO_2, accompanied by other oxidized species and that the presence of nitrogen induce the formation of non negligible amounts of oxygen vacancies (Vo) and reduced Sn^{2+} species.

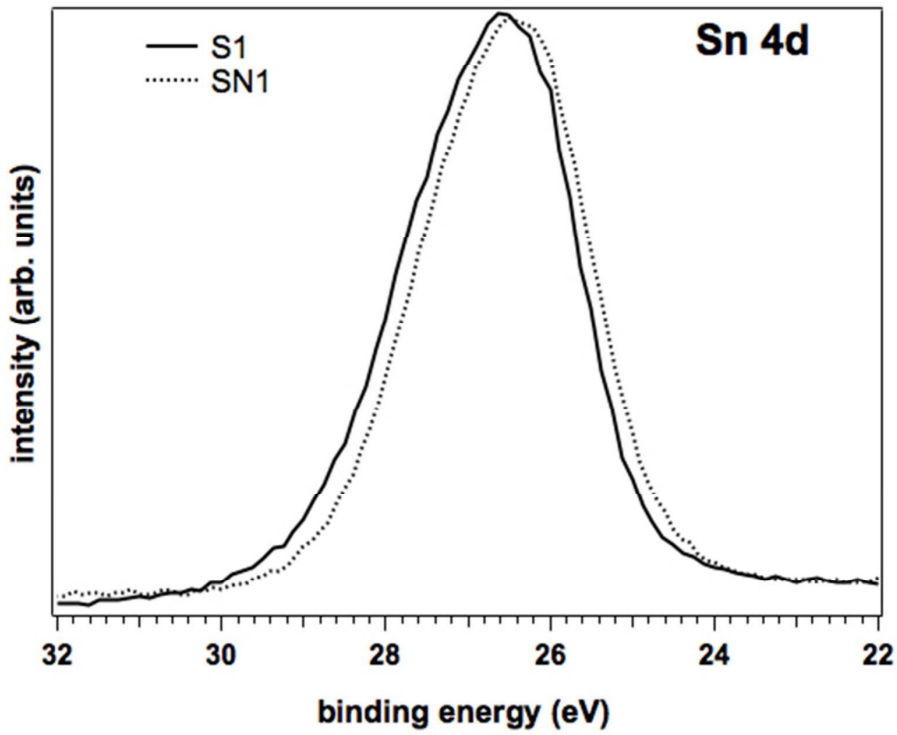

Fig. 7 XPS data of Sn (4d) of S1 (undoped) and SN1 (nitrogen doped).

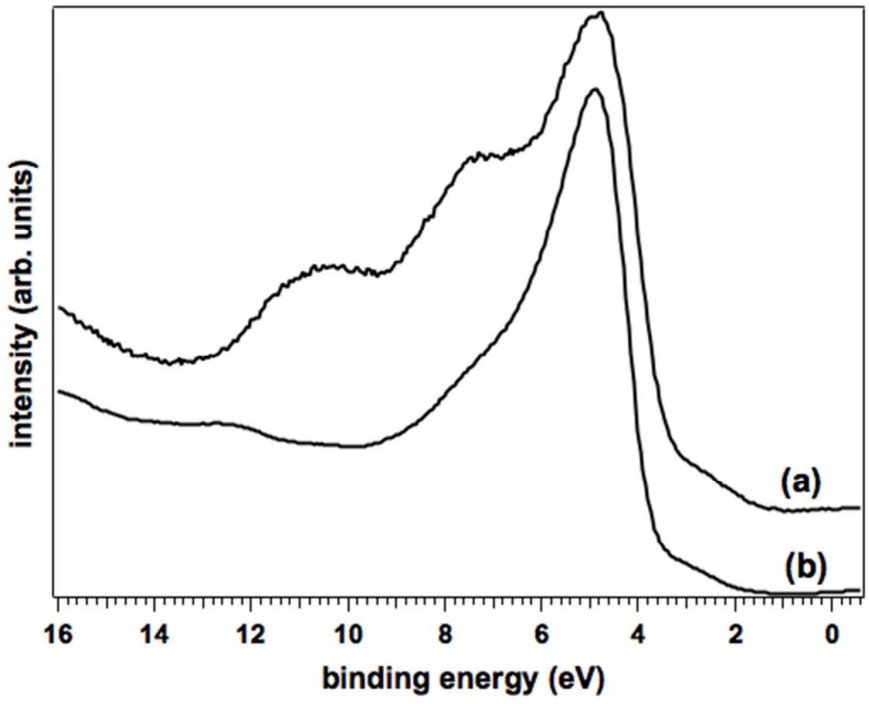

Fig. 8 UPS data of SN1 sample obtained with two He emission (He(II) = 40.8 eV, He(I) = 21.2 eV).

4. Discussion.

The preparation methods adopted in this work easily allow to introduce nitrogen in the SnO_2 lattice whose properties (optical, electronic and textural) are markedly influenced by the doping. The well-known sensitiveness of SnO_2 stoichiometry to the external conditions, namely temperature and oxygen partial pressure, that is favoured by the dual oxidation state of tin, is even accentuated by the inclusion of nitrogen in the lattice as indicated by all the experimental techniques employed in the present work (UV-Vis-NIR, EPR and XPS).

4.1 Nitrogen containing species in N-SnO_2.

Inspection of XPS data and analysis by deconvolution of N 1s peak allows the identification of several components indicating the presence in the solid or at its surface of different nitrogen containing species. These can be divided in two families. The former one, corresponding to the two components at 397.1eV and 398.3 eV is associated to Sn-N-Sn bonds where nitrogen gives rise to a nitride centre with N directly bridging metal centers. Each component corresponds to a slightly different environment.[55] The remaining peaks between 399.4 eV and 403.2 eV can be ascribed to different types of neutral or charged NO_x fragments. The XPS results are in broad agreement with those from EPR which clearly identify two nitrogen containing species. The first one, molecular trapped NO, corresponds to one of the XPS peaks at higher binding energy. As it occurs for other semiconducting oxides[44] NO and other N containing species (NH_4^+, CN^-, NO_2^-) are by-products of the synthesis performed using ammonia often found at the extreme surface of the solid. Usually such species have no direct influence on the electronic structure of the doped solid and will not be discussed further in the present paper.

More relevant for the properties of N-SnO_2 is the second EPR active species (species B, N_{sub}) whose EPR spectrum has been thoroughly analyzed in a previous paper[32] by comparison between experimental and computed hyperfine parameters. In short this analysis indicates that the unpaired electron is located in a N 2p orbital weakly delocalized onto three equivalent Sn. This has allowed to describe this paramagnetic entity in terms of a "substitutional" center with nitrogen

replacing oxygen in the SnO_2 crystallographic position. The paramagnetic centre can be formally described as a tri-coordinated N^{2-} ion, a 7 electrons centre that can be seen as a nitride (N^{3-}) ion trapping a hole. In analogy to what has been observed in the case of TiO_2, such a centre can easily scavenge electrons with higher energy transforming into the diamagnetic, EPR silent, N^{3-}. The EPR data discussed in Section 3.5 indicate that N^{2-} is observed when the system is fully oxidized (hence electron-poor). The gradual (and reversible) disappearance of the signal which accompanies the spontaneous oxygen depletion (Fig. 3) is indeed due to the mentioned process:

5) $N^{2-} + e^- \boxtimes N^{3-}$

N^{2-} and N^{3-} coexists in N-SnO_2 in various mutual ratios depending on the oxidation degree of the solid and are monitored by XPS in terms of the N 1s XPS signal at lower binding energy (see Section 3.1).

4.2 Electronic structure of N-SnO_2

Once established that N-SnO_2 differs from bare SnO_2 for the presence of nitride-type centers the attention must be paid to the effects of doping on the electronic structure of the oxide. This can be done comparing the UV-Vis-NIR spectra with the UPS results. In terms of optical absorption (Fig. 2) three main features make N-SnO_2 different from the undoped oxide, namely: *i)* a weak red shift of the band gap transition; *ii)* a tail of this transition towards the visible region (responsible of the color) and *iii)* a more pronounced drift of the absorption in the NIR region .

A detailed analysis of the bandgap value is not possible on the basis of the present data also because of the influence that the Burstein-Moss effect has on this parameter. However, it is worth noting that the magnitude of such shift is not enough to justify the visible light absorption. More relevant to our discussion is point *ii)* i.e. the absorption in the visible region (Fig. 2, panels B and B') that is related to the presence of low energy states close to the top of the valence band. This assertion is possible on the basis of a comparison between the optical absorption and the valence band UPS spectra of as-prepared N-SnO_2 (Fig. 6e) that clearly show a shoulder at about 2 eV. This feature

monitors the low-lying states resulting from the hybridisation of oxygen p-orbitals with (occupied) 5s states of tin[53] and is more intense in the case of the doped material compared to the bare SnO_2 after the same calcination treatment. As-prepared N-SnO_2 is rich of reduced Sn(II) states that form, with similar concentration in undoped SnO_2, only upon a prolonged reductive annealing. These Sn(II) states (and not the N ones) are responsible of the yellow colour of N-SnO_2. Note that a similar colour is shown by particular SnO_2 materials, non-containing N, but simply "self-doped" with Sn^{2+}.[8,9,10,56,57]

The presence of excess electrons in the form of Sn(II) centres is also accompanied by that of other electrons in the conduction band (Fig. 2, C and C')

This indicates that, in spite the fact that the nitrogen doped system should be a p-doped oxide (it possesses low-lying nitrogen hole centers), this is still compensated by a rich density of electrons stemming from its non stoichiometry, consequently preserving its resilient n-type character. The n-type properties of N-SnO_2, suggested by the optical behavior in Fig. 2, are fully confirmed by photoelectron spectroscopy. In particular in the UPS spectrum in Fig. 6 the valence band maximum is observed at 3.4 eV (3.0 only in the case of pristine SnO_2). Since the band gap energy of the solid is around 3.6-3.8 eV, the VBM value firmly point to a pinning of the Fermi level just underneath the conduction band as it occurs in n-type systems. The anomaly of the doped system has to be explained in terms of the higher propensity of N-SnO_2 , with respect to SnO_2, to form oxygen vacancies releasing O_2 similarly to what has been reported for the N-TiO_2 system where the energetic cost to produce an oxygen vacancy is dramatically reduced if N is included in the lattice.[58,59] The low-lying empty states of nitrogen (hole states) in fact becomes efficient scavengers (equation 5) for the electrons left in the solid subsequently to the oxygen release (equation 1), contributing to lower the whole electronic energy of the defective system. The same mechanism observed for TiO_2 is likely operating in SnO_2 when low energy N hole states (N^{2-}) are present in the lattice. The extra electrons left in the solid are in part stabilized at low energy under the form of N^{3-} and Sn(II) centers and in part remain in the oxygen vacancy from which they are easily ionized into

the CB. This description seems to be the only one taking into account the whole set of experimental evidences reported in this paper confirming the paradoxical view of a potential p-type doped system that still retain an n-type character even higher than the undoped one as suggested by the comparison of the NIR absorption shown in Fig. 2 C and C'. A qualitative comparison between the electronic structure of SnO_2 and N-SnO_2 is proposed in Fig 9. Further evidence should be useful to confirm the above picture (from conductivity measurements to computations of the energetic cost of vacancy formation). However, the data collected in this work resolutely point in the described direction leaving therefore little hope for the preparation of a p-type SnO_2 via nitrogen doping.

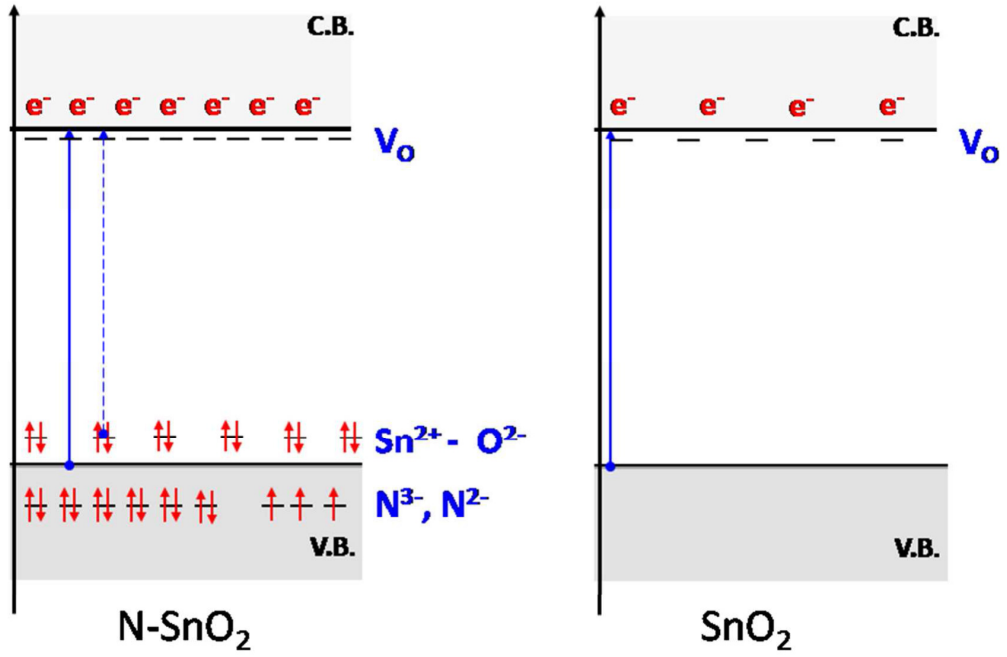

Fig. 9. Sketch reporting a schematic view of the main electronic features of Nitrogen doped SnO_2 (N-SnO_2) and prisitne SnO_2.

5. Conclusion.

Nitrogen doped SnO_2 in the form of nanometric powders has been successfully prepared via precipitation methods using ammonia playing both roles of precipitating agent and of nitrogen source.

The doping procedure has led to the formation (beside several by-products of the preparation) of a defect center (never observed before) consisting in a nitrogen atom substituting an oxygen of the SnO_2 lattice. Two forms of this nitride-like center exist either paramagnetic (N^{2-}) or diamagnetic (N^{3-}), for which the ratio depends on the oxidation state of the solid. The energy of the SOMO and HOMO orbitals of the two kinds of nitride centers lies in the valence band energy range. The doped material is yellow colored because of the transitions caused by the presence of low-lying Sn(II) states above to the VB maximum. Moreover, even though the nitrogen potentially represents a p dopant for semiconducting oxide, the N doped material prepared in this work is still rich of excess electrons as a result of its higher propensity to lose oxygen that is, in turn, determined by the presence of low lying N states in the band structure. This evidence also suggests that the chance to prepare a p-type form of tin oxide, at least via nitrogen doping, is extremely low.

Acknowledgments

This work has been supported by the CARIPLO Fondation through the grant n° 2013-0615 "Novel heterojunction based photocatalytic materials for solar energy conversion" and by the Italian MIUR through the FIRB Project RBAP115AYN “Oxides at the nanoscale: multifunctionality and applications”. The support of the COST Action CM1104 “Reducible oxide chemistry, structure and functions” is also gratefully acknowledged. NB and FS wish to acknowledge Dr. Carine Davoisne (LRCS) for transmission electron microscopy investigation on SnO_2 and N-SnO_2.

References.

[1] M. Batzill, U. Diebold, *Prog. Surf. Sci.* 2005, **79**, 47-154.

[2] Ç. Kılıç, A. Zunger, *Phys. Rev. Lett.* 2002, **88**, 095501-4.

[3] S. Das, V. Jayaraman, *Prog. Mater. Sci.* 2014, **66**, 112–255.

[4] Y. Idota, T. Kubota, A. Matsufuji, Y. Maekawa, T. Miyasaka, *Science* 1997, **276**, 1395-1397.

[5] S. Gubbala, V. Chakrapani, V. Kumar, M.K. Sunkara, *Adv. Funct. Mater.* 2008, **18**, 2411-2418.

[6] P.G. Harrison, C. Bailey, W. Azelee, *J. Catal.* 1999, **186***,* 147-159.

[7] A. Enesca, L. Isac, L. Andronic, D. Perniu, A. Duta, *Appl. Catal. B* 2014, *147*, 175-184.

[8] C-M. Fan, Y. Peng, Q. Zhu, L. Lin, R-X. Wang, A-W. Xu *J. Phys. Chem. C* 2013, **117**, 24157−24166.

[9] H. Wang, K. Dou, W.Y. Teoh, Y. Zhan, T. F. Hung, F. Zhang, J. Xu, R. Zhang, A.L. Rogach, *Adv. Funct. Mater.* 2013, **23**, 4847–4853.

[10] M. Sun, Y. Su, C. Du, Q. Zhao, Z. Liu, *RSC Adv.* 2014, **4**, 30820–30827.

[11] T. Nutz, U. Felde, M. Haase, *J. Chem. Phys.* 1999, **110**, 12142-12150.

[12] T. Nutz, M. Haase, *J. Phys. Chem. B* 2000**, 104***,* 8430-8437.

[13] E. Elangovan, K. Ramamurthi, *Appl. Surf. Sci.* 2005, **249**, 183–196.

[14] H. Kim, R.C.Y. Auyeung, A. Piqué, *Thin Solid Films* 2008, **516**, 5052–5056.

[15] G. Barolo, S. Livraghi, M. Chiesa, M.C. Paganini, E. Giamello, *J. Phys. Chem. C,* 2012, **116**, 20887-20894.

[16] F. Napoli, M. Chiesa, E. Giamello, M. Fittipaldi, C. Di Valentin, F. Gallino, G. Pacchioni, *J. Phys. Chem. C,* 2010, **114**, 5181-5192.

[17] Y. Yan, S. B. Zhang, S.T. *Phys. Rev. B* 2001, **96**, 5723-5726.

[18] S.S. Pan, C. Ye, X.M. Teng, H.T. Fan, G.H. Li, *Appl. Phys. A* 2006, **85**, 21–24.

[19] S.S. Pan, C. Ye, X.M. Teng, L. Li, G.H. Li, *App. Phys. Lett.* 2006, **89**, 251911-3.

[20] S. Luo, P.K. Chu, Z. Di, M. Zhang, W. Liu, C. Lin, J. Fan, Wu, X. *App. Phys. Lett.* 2006, **88**, 013109-3.

[21] X. Sun, R. Long, X. Cheng, X. Zhao, Y. Dai, B. *J. Phys. Chem. C* 2008, **112***,* 9861–9864.

[22] S.S. Pan, G.H. Li, L.B. Wang, Y.D. Shen, Y. Wang, T. Mei, X. Hu, *App. Phys. Lett.* 2009, **95**, 222112-3.

[23] R.; Long, N.J. English, *Phys. Lett. A* 2009, **374***,* 319–322.

[24] W-Z. Xiao, L-L. Wang, L. Xu, Q. Wan, B.S. Zou, *Solid State Commun.* 2009, **149**, 1304-1307.

[25] G.X. Zhou, S.J. Xiong, X.L. Wu, L.Z. Liu, T.H. Li, P.K. Chu, *Acta Mater.* 2013, **61**, 7342–7347.

[26] X. Ding, F. Fang, J. Jiang, *e-J. Surf. Sci. Nanotechnol.* 2013, **231**, 67–70.

[27] N. Wan, T. Zhao, S. Sun, Q. Wu, Y. Bai, *Electrochim. Acta* 2014, **143**, 257–264.

[28] B. Zhou, S. Dong, H. Zhao, Y. Liu, P. Wu, *J. Magn. Magn. Mater.* 2014, **362**, 14–19.

[29] N. Wan, P. Yu, S. Sun, Q. Wu, T. Li, Y. Bai, *Mater. Lett*. 2014, **133**, 168–170.

[30] M. Ara, V.R. Chitturi, S.O. Salley, K.Y.S. Ng, *Electrochim. Acta* 2015, **161**, 269-278.

[31] A.; Nouri, A. Fakhri, *Spectrochim. Acta Part A* 2015, **138**, 563–568.

[32] E. Albanese, C. Di Valentin, G. Pacchioni, F. Sauvage, S. Livraghi, E. Giamello. *J. Phys. Chem. C* 2015, **119**, 26895-26903.

[33] D.O. Scanlon, G.W. Watson, J. Mater. Chem. 2012, **22**, 25236–25245

[34] M. Radecka, M. Rekas, A. Trenczek-Zajac, K. Zakrzewska, *J. Power Source*s 2008, **181**, 46–55.

[35] A.S. Ahmed, A. Azam, M.M. Shafeeq, M. Chaman, S. *J. Phys. Chem. Solids* 2012, **73**, 943–947.

[36] S. Patra, C. Davoisne, H. Bouyanfif, D. Foix, F. Sauvage, *Sci. Rep.* 2015, **5**, 10928-10938.

[37] G. Sanon, R. Rup, A. Mansingh, *Phys. Rev. B* 1991, **44**, 5672-5680.

[38] J. Biedrzycki, S. Livraghi, E. Giamello, S. Agnoli, G. Granozzi, *J. Phys. Chem. C* 2014, **118**, 8462−8473.

[39] A.K. Chandirian, F. Sauvage, M. Casas-Cabanas, P. Comte, M. Grwetze, *J. Phys. Chem. C* 2010, **37**, 15849-15856.

[40] A.H. Kahn, *Phys. Rev.* 1955, ***97***, 1647-1652.

[41] C. Di Valentin, G. Pacchioni, M. Chiesa, E. Giamello, S. Abbet, U. Heiz, *J. Phys. Chem. B* 2002, **106**, 1637-1645.

[42] S. Livraghi, M.C. Paganini, M. Chiesa, E. Giamello, *Res. Chem. Intermed.* 2007, **33**, 739-747.

[43] S. Morandi, M.C. Paganini, E. Giamello, M. Bini, D. Capsoni, V. Massarotti, G. Ghiotti, *J. Solid State Chem.* 2009, **182**, 3342–3352.

[44] S. Livraghi, M.R. Chierotti, E. Giamello, G. Magnacca, M.C. Paganini, G. Cappelletti, C.L. Bianchi, *J. Phys. Chem. C* 2008, **112**, 17244-17252

[45] M. Primet, M. Che, C. Naccache, M-V. Mathieu, B. Imelik, *J. Chim. Phys. Phys.- Chim. Biol.* 1970, **67**, 1629-1635.

[46] M. Niwa, T. Minami, H. Kodama, T. Hattori, Y. Murakami, *J. Catal.* 1978, **53**, 198-207.

[47] Y. Mizokawa, S. Nakamura, *Jap. J. App. Phys*. 1975, **14**, 779-788.

[48] C. Canevali, C.M. Mari, M. Mattoni, F.;Morazzoni, R. Ruffo, R. Scotti, U.;Russo, L. *Sens. Actuators B* 2004, **100**, 228–235.

[49] M. D'Arienzo, D. Cristofori, R. Scotti, F. Morazzoni, *Chem. Mater.* 2013, **25**, 3675−3686.

[50] S. Livraghi, M.C. Paganini, E. Giamello, A. Selloni, C. Di Valentin, G. Pacchioni, *J. Am. Chem. Soc.* 2006, **128**, 15666−15671.

[51] D. Lützenkirchen-Hecht, R. Frahm, *Thin Solid Films* 2005, **493**, 6–76.

[52] Y. Inoue, M. Nomiya, O.Takai, *Vacuum* 1998, **51**, 673-676.

[53] J-M. Themlin, M. Chtaib, L. Henrard, P. Lambin, J. Darville, J-M. Gilles, *Phys. Rev. B* 1992, **46**, 2460-2466.

[54] J.J. Yeh, I. Lindau, *Atomic Data and Nuclear Data Tables*, 1985, **32**, 1-155.

[55] F E. Oropeza, J. Harmer, R.G. Egdell, R.G. Palgrave, *Phys. Chem. Chem. Phys.* 2010, **12**, 960–969.

[56] N. Li, K. Du, G. Liu, Y. Xie, G. Zhou, J. Zhu, F. Li, H-M. *J. Mater. Chem. A* 2013, **1**, 1536-1539.

[57] V.B. Kamble, A.M. Umarji, *AIP Adv.* 2013, **3**, 082120-5.

[58] C. Di Valentin, G. Pacchioni, A. Selloni, S. Livraghi, E. Giamello, *J. Phys. Chem. B,* 2005, **109**, 11414-11419.

[59] M. Batzill, E.H. Morales, *Phys. Rev. Lett.* 2006, **96**, 026103

T.O.C.

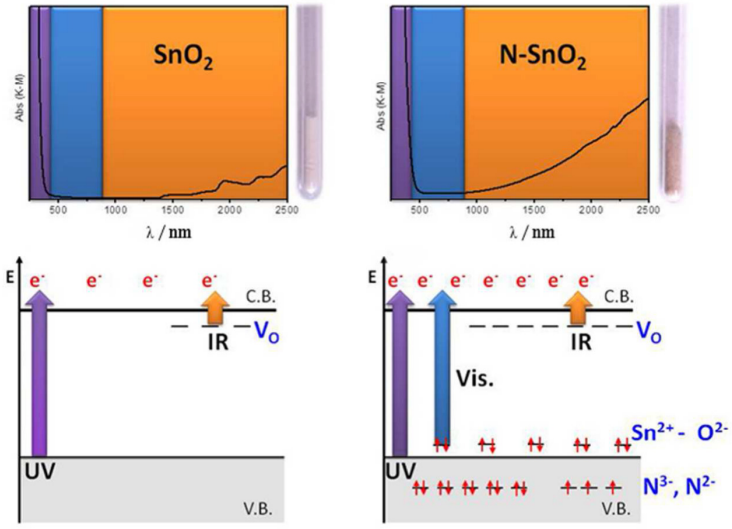

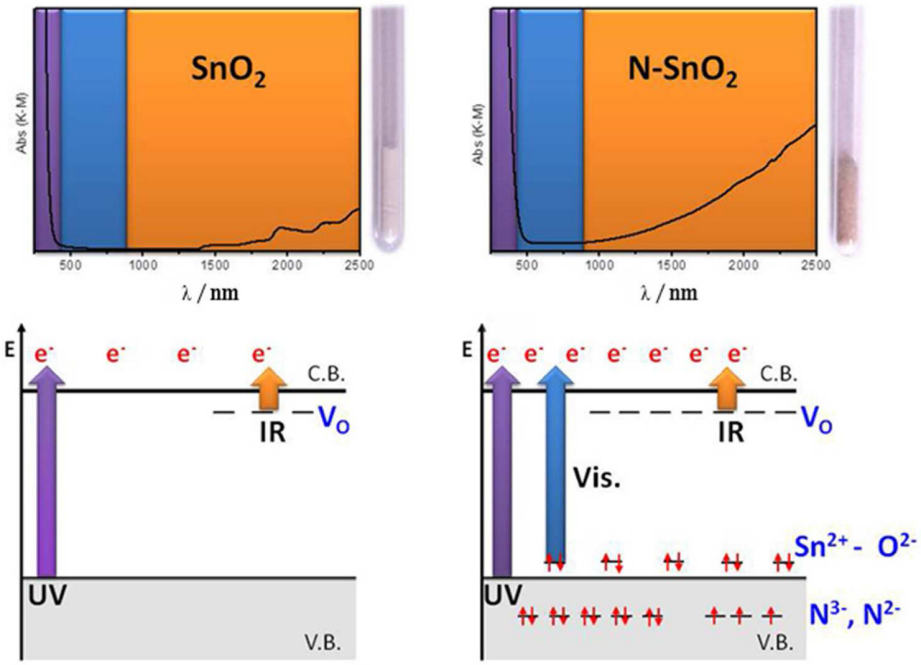

57x43mm (300 x 300 DPI)